Am J Cancer Res 2026;16(11):4815-4832
www.ajcr.us /ISSN:2156-6976/ajcr0174644

Original Article

p53-activated miR-4286 targets *SNAI1* and suppresses malignant phenotypes in endometrial cancer

Litong Zhu[1,2,3*], Yubing Hu[1,4*], Aiqi Yin[2*], Caiqiu Xu[2], Yanyi Xiao[5], Ping Jin[1,3,4], Suiqun Guo[2]

[1]Department of Gynecology, Shenzhen Maternity and Child Healthcare Hospital, Women and Children's Medical Center, Southern Medical University, Shenzhen 518047, Guangdong, China; [2]Department of Obstetrics and Gynecology, The Third Affiliated Hospital of Southern Medical University, Guangzhou 510315, Guangdong, China; [3]State Key Laboratory of Ultrasound in Medicine and Engineering, College of Biomedical Engineering, Chongqing Medical University, Chongqing 400016, China; [4]Shenzhen School of Clinical Medicine, Southern Medical University, Shenzhen 518000, Guangdong, China; [5]Reproductive Medicine Center, The First Affiliated Hospital, Sun Yat-sen University, Guangdong Provincial Key Laboratory of Reproductive Medicine, Guangzhou 510080, Guangdong, China. [*]Co-first authors.

Received June 10, 2026; Accepted October 25, 2026; Epub November 15, 2026; Published November 30, 2026

Abstract: MicroRNAs (miRNAs/miRs) play key regulatory roles in cancer progression. Previous investigations have identified miR-4286 as either a promoter or a suppressor of cancer and implicated it in tumor pathogenesis. However, its specific role in endometrial cancer (EC) remains unexplored. This study aimed to investigate the molecular mechanisms underlying miR-4286 and evaluate its influence on proliferation, invasion, and metastasis in EC. We detected reduced miR-4286 expression in EC samples using *in situ* hybridization assays. Kaplan-Meier survival analyses revealed that miR-4286 served as a favorable factor in EC. Experimental data showed that miR-4286 exerted an obvious antitumor effect *in vitro* and *in vivo*, and had a significant impact on the biological functions of EC cells. Mechanistically, we found that p53 directly bound to the promoter region of miR-4286 to drive its transcription, whereas miR-4286 directly targeted the 3'-untranslated region of *SNAI1* mRNA to repress SNAI1 expression. Consequently, the p53/miR-4286/SNAI1 axis inhibited the epithelial-mesenchymal transition, accompanied by reduced levels of phosphorylated PI3K and Akt in EC cells. In conclusion, this study was novel in demonstrating that miR-4286 served as a potential biomarker and played a crucial tumor-suppressive role in EC pathogenesis.

Keywords: EMT, endometrial cancer, miR-4286, PI3K/Akt, *SNAI1*

Introduction

Endometrial cancer (EC) is the second most prevalent gynecological malignancy, with a steadily increasing number of new cases diagnosed. Between 2013 and 2022, the incidence of EC exhibited an annual growth rate of approximately 1%, whereas the mortality rates increased at a more alarming rate of 1.5% [1]. This disease poses a significant threat to women's health and contributes substantially to the medical and social burdens on society. The Cancer Genome Atlas (TCGA) classified EC into four distinct molecular subtypes: POLE (polymerase epsilon)-mutated, mismatch repair deficient, copy-number low, and copy-number high. These subtypes offer novel perspectives on diagnostic, prognostic, and therapeutic targets for EC tumors [2]. Despite advancements in treatment, the disease prognosis and recurrence rates for certain patients with EC remain poor, leading to a decrease in EC survival over the past four decades [3]. Therefore, the molecular mechanisms underlying EC pathogenesis require comprehensive investigation to identify new molecular targets for improved EC diagnostics and therapy.

MicroRNAs (miRNAs), which are short noncoding RNA molecules ranging from 18 to 25 nucleotides in length, play a crucial role in regulating various cellular processes. These encompass cell proliferation, differentiation, apoptosis, cell cycle regulation, tissue development, and regeneration processes [4]. Recently, several miRNA-targeted therapeutics progressed from

https://doi.org/10.62347/ZOTM4194

bench to bedside, including miR-21 (phase I clinical trials) and miR-124 (phase II trials) [5, 6]. As miRNAs regulate gene expression and protein output, they can be used in cancer therapeutics. A previous study identified miR-4286 as either a promoter or a suppressor of cancer and implicated it in tumor pathogenesis because it mediated prostate cancer cell proliferation and apoptosis [7]. The molecule was also an unfavorable prognostic marker for metastatic melanoma [8]. Moreover, miR-4286 functioned as a tumor suppressor by targeting both transforming growth factor B1 (TGFB1) and TGFBR2, thereby regulating TGF-β signaling in glioblastoma multiforme [9]. Nonetheless, the role and significance of miR-4286 in EC remain inadequately understood.

This study investigated the molecular mechanisms underlying miR-4286 and evaluated its influence on the proliferation, invasion, and metastasis in EC. Our findings indicated that p53 activated miR-4286 and miR-4286 functioned as a tumor suppressor by targeting *SNAI1*. We also observed changes in epithelial-mesenchymal transition (EMT)-associated protein and phosphorylated PI3K and Akt levels expression following miR-4286 modulation.

Methods

Cell culture

HEC-1-B (*TP53*-mutant) and RL95-2 (*TP53* wild-type) EC cell lines, along with HEK293T human embryonic kidney cells, were used in this study. All these cell lines were generously provided by the Cell Bank of the Chinese Academy of Sciences. For cell culture, DMEM with high glucose (Hyclone, USA) was employed, and the medium was augmented with 10% FBS (ExCell, Shanghai, China). The cells were incubated at 37°C with 5% carbon dioxide and suitable humidity to ensure optimal growth conditions.

Collection of clinical samples

Tissue microarrays (TMAs) HUteA060CS01 and EMC1351 were purchased from Shanghai Outdo Biotech Company (China). HUteA060-CS01 included 34 EC and 26 adjacent normal endometrial specimens. EMC1351 included 118 EC, with their survival follow-up time, and 17 adjacent normal endometrial specimens. Given the retrospective nature of the TMA, detailed treatment regimens, TCGA molecular classifications, and hormonal status (ER/PR) were not available. Approval for research involving human tissue was obtained from the Shanghai Outdo Biotech Company (ethics approval No. YB M-05-02). The specimens were validated through a pathological diagnosis and staged according to the 2018 FIGO classification.

Cell transfection

This study sourced the *TP53* expression plasmid from Vigene BioSciences (Shandong, China). Guangzhou Ruibo Biotechnology Co., Ltd. designed and synthesized miR-4286 mimics, miR-4286 inhibitors, and small interfering RNA (siRNA) targeting *SNAI1*. The related sequence details are provided in Table S1. HEC-1-B and RL95-2 EC cell lines were seeded in 6-well (2×10^5/well for HEC-1-B and 2.5×10^5/well for RL95-2) or 96-well (2000/well for HEC-1-B and 3000/well for RL95-2) plates (Nest Biotech, USA) for approximately 24 h. The cells were transfected when the confluency levels ranged from 30% to 50%. The transfection process used Lipofectamine 2000 reagent (Invitrogen, USA) and was performed in Opti-MEM from Gibco (USA). The cells were collected for further experimental analyses between 48 and 72 h after transfection.

RNA extraction and reverse transcription

Total RNA was extracted from EC cells using TRIzol reagent (TaKaRa, Japan). The extracted RNA was converted into cDNA using the reverse transcription kit (TaKaRa).

Real-time quantitative polymerase chain reaction

The synthesized cDNA served as a template in real-time quantitative polymerase chain reaction (qRT-PCR) and was amplified with specific primer pairs. These primers were designed for mRNA and miRNA. The detailed sequence information is shown in Table S2. U6 small nuclear RNA was used as the internal control for miRNA expression (miR-4286). *p14ARF* was used as the internal reference gene for mRNA expression analysis in these experiments. The qRT-PCR was conducted strictly following the standard procedures provided by TaKaRa Bio

Inc. (Shiga, Japan). The experiment was performed independently three times to achieve significant differences in data.

Western blotting

The protein levels were assessed using Western blotting following previously established methodology [10]. The primary antibodies used in the experiment included PI3K, p-PI3K, Akt, p-Akt, p21, E-cadherin, N-cadherin, Vimentin, Snail, and Slug. Also, GAPDH and β-actin served as internal controls. The source and dilution ratio of related antibodies are shown in Table S3. The membranes were incubated with primary antibodies against targeted proteins overnight at 4°C with gentle shaking. Following three washes with TBST, the membranes were incubated with horseradish peroxidase-conjugated secondary antibodies at 37°C for 1 h. The blot images were visualized using enhanced chemiluminescence reagent (SinSage Technology Co., Ltd., Beijing, China). The band intensity was quantified using ImageJ software. The gray mean value of each band was measured. The relative expression levels of the target proteins were normalized to the internal reference protein (GAPDH or β-actin). The results were expressed as the fold change relative to the control group.

Cell proliferation assay

Following the transient transfection of EC cells with miR-4286 mimetic or inhibitor, 2000-3000 cells/well were seeded into 96-well plates. After cell culturing for 4 days, 20 μL of MTT solution (Sigma Corporation, USA) was added to each well for 4 h. At this point, the metabolically active cells produced formazan crystals. Subsequently, 150 μL of dimethyl sulfoxide (Sigma Corporation) was added to dissolve the crystals, and then the absorbance value was determined at 490 nm using a microplate reader (BioTek Instruments, USA). The reproducibility of the experimental results was ensured by conducting all experiments three times independently.

5-Ethynyl-2'-deoxyuridine incorporation assay

A 5-Ethynyl-2'-deoxyuridine (EdU) labeling approach was employed to assess cell proliferation using Apollo567 *in vitro* imaging kit (RiboBio Co., Ltd., China). First, the treated cells were inoculated in a culture medium with 10 mM EdU and incubated for 2 h, enabling the incorporation of the thymidine analog EdU into the newly synthesized DNA strand during the cell DNA synthesis phase (S phase). Next, the cells were fixed with 4% paraformaldehyde to preserve their morphological structure. After fixation, a 0.3% Triton X-100 solution was used to permeabilize the cell membrane, laying the groundwork for the subsequent penetration of staining reagents. Then, Apollo567 fluorescent dye was used to specifically mark the incorporated EdU; the reaction was conducted in the dark. For distinct visualization, the nucleus was stained with 5 μg/mL 4', 6-diamidino-2-phenylindole for 10 min and observed under a fluorescence microscope (Olympus, Japan). Five fields were randomly chosen, and the cell proliferation rate was computed. All experiments were repeated independently three times.

In vitro cell migration and invasion assays

In this study, a Transwell chamber (Corning Incorporated, NY, USA) was used to conduct the migration experiment. The treated EC cells were placed in serum-free medium and incubated for 24 h for starvation. Then, 100 μL of cell suspension was added to each well, and 500 μL of culture medium with 10% FBS was added to the lower chamber. After culturing for 10-12 h, the cells that migrated to the lower surface of the Transwell membrane were subjected to Giemsa staining and then counted under a microscope. For the invasion assay, the Transwell chambers were pre-coated with Matrigel (Corning, USA) to perform the Boyden chamber-based invasion assay. The operational steps were analogous to those of the migration experiment. All experiments were repeated independently three times.

In vivo tumorigenesis assays

Ten 4-week-old female BALB/c nude mice were obtained from Nanjing University, located in Jiangsu Province, China. For *in vivo* tumorigenesis assay, 4×10^6 EC cells were administered subcutaneously into the lateral abdomen of the mice, with each EC cell line allocated to five mice. After 8 days, the tumor tissue on the left side was injected with 1 nmol negative control micrON agomir (RiboBio) in 10 μL of sterile saline every 3 days via multipoint intra-

tumoral injection, whereas the tumor tissue on the right side was injected with 1 nmol micrON agomir-4286 (RiboBio). The mice were kept in specific pathogen-free conditions. After 4 weeks, the mice were anesthetized with sodium pentobarbital and humanely euthanized via cervical dislocation, in strict accordance with the ARRIVE guidelines. Tumor xenografts were removed and weighed.

The animal experiments in this study strictly adhered to the pertinent principles and protocols outlined in the Guide for the Care and Use of Laboratory Animals of Southern Medical University, with the experimental license number SCXK (Guangdong) 2008-0002.

In vivo metastasis assays

Twelve 4-week-old female BALB/c nude mice were purchased from Nanjing University, Jiangsu Province. For *in vivo* metastasis assays, 1×10^6 EC cells were injected into nude mice through the liver capsule, with each EC cell line corresponding to six nude mice. After 8 days, the mice in the first group were intraperitoneally injected with 1 nmol micrON agomir-control (RiboBio) in 20 μL of sterile saline every 3 days. In the second group, the mice received 1 nmol micrON agomir-4286 (RiboBio). The mice were anesthetized via intraperitoneal injection of sodium pentobarbital (50 mg/kg). Following an upper-left abdominal incision to expose the liver, 30 μL of a cell suspension containing 1×10^6 EC cells was slowly injected beneath the hepatic capsule. To prevent cell leakage and achieve complete hemostasis, a sterile cotton swab was applied over the injection site with gentle pressure for 2 min. The abdominal incision was then sutured in layers. Postoperatively, the mice were placed on a warming pad until they fully recovered from anesthesia and monitored daily for body weight and general health. After 40 days, the mice were humanely euthanized via cervical dislocation following sodium pentobarbital anesthesia, in strict accordance with the ARRIVE guidelines. The tumor tissues were collected for analyses.

Immunohistochemical staining

Immunohistochemical (IHC) detection was used to analyze the protein expression of Snail, Ki67, proliferating cell nuclear antigen (PCNA), E-cadherin, and N-cadherin. The procedure was carried out using previously reported methods [11]. The antibodies used included anti-Snail, Ki67, PCNA, E-cadherin, and N-cadherin antibodies (Table S3). For each staining, isotype-matched normal immunoglobulin G (IgG) was used as a negative control in place of the primary antibody.

Chromatin immunoprecipitation assay

Based on bioinformatics predictions from the JASPAR database, three potential p53-binding sites were found in the promoter region of miR-4286. To verify this prediction, chromatin immunoprecipitation (ChIP) was carried out using a Pierce Agarose ChIP kit (Thermo Fisher Scientific), combined with anti-p53 and IgG antibodies, following the kit instructions. The specific steps were as follows: *TP53*-transfected EC cells were fixed with 1% formaldehyde for covalent cross-linking of proteins with DNA, and then the cell chromatin was collected. The cross-linked DNA was fragmented by ultrasonic treatment to obtain fragments of 200-1000 base pairs. The p53-DNA complex was immunoprecipitated with specific antibody. Finally, the chromatin fragment specifically binding to the miR-4286 promoter region was verified by PCR amplification and agarose gel electrophoresis.

Electrophoretic mobility shift assay

The electrophoretic mobility shift assay (EMSA) kit (Guangzhou Bosen Biotechnology Co., Ltd.) was used to detect the binding of the p53 protein to the miR-4286 promoter region. The specific EMSA probe for miR-4286 was designed and synthesized by the company. EMSA was carried out as previously reported [12]. The binding reaction system contained 1.5 μL of binding reagent, 1 μL of poly (dI:dC), 5 μL of nuclear extract, 5 μL of biotin-labeled probe, and a hundredfold molar excess of unlabeled wild-type or mutant *TP53* oligonucleotide competitors. The reaction was carried out at room temperature for 20 min. A negative control was established using EC cell extract devoid of nucleoprotein, whereas an anti-p53 antibody served as a control for the supermigration band. Following the reaction, an enhanced chemiluminescence reagent was employed to detect and stabilize the target band.

Luciferase reporter assay

To clarify the targeted regulatory interplay between miR-4286 and the *SNAI1* gene, the potential binding sites were predicted using bioinformatics analysis tools such as TargetScan and RNAhybrid. Based on the prediction outcomes, the 3'-untranslated region (3'-UTR) fragment of the *SNAI1* gene, containing the wild-type binding sequence of miR-4286 and its mutant sequence, was synthesized and inserted into the psiCHECK-2 reporter vector (Promega Corporation, USA). Consequently, the constructed wild-type or mutant reporter plasmid was co-transfected into HEK293T cells along with miR-4286 mimetic or inhibitor. The transfection was performed using Hieff Trans liposome transfection reagent (Yisheng Biotechnology Co., Ltd., China). The group transfected with the psiCHECK-2 empty vector and the group transfected solely with miR-4286 mimetic or inhibitor served as negative controls. The luciferase activity of cells in each group was measured using the dual-luciferase reporter system to assess the direct regulatory effect of miR-4286 on the 3'-UTR of the *SNAI1* gene.

Dual-luciferase reporter assay

The *TP53*-binding site fragment was PCR-amplified and inserted into a psiCHECK-2 luciferase reporter plasmid to generate a miR-4286 promoter plasmid. Also, *TP53*-binding site mutation plasmids were constructed. Wild-type or mutant reporter plasmids were co-transfected into HEK293T cells. After a 48-h transfection, the luciferase activity was measured.

In situ hybridization

A set of standardized procedures was performed on EC tissue microarrays (EC TMAs). Initially, the sample underwent dewaxing with xylene, followed by hydration using a decreasing concentration gradient of ethanol solutions. Then, the sample was processed in a 0.1% hydrochloric acid solution for 15 min. Next, the TMA was placed at 37°C, incubated with 3% fresh citrate buffer containing diluted pepsin for 20 min, and rinsed with phosphate-buffered saline. The pre-hybridization steps were as follows: First, the pre-hybridization solution was incubated at 37°C for 2 h and then hybridized with a digoxigenin (DIG)-labeled locked nucleic acid probe targeting the mature human miR-4286 sequence (miRBase Accession No. MIMAT0016916; supplied by Biochem Pharmaceuticals Industries) at 37°C for 22 h. After hybridization, the samples were subjected to gradient washing: First, with 2 × SSC solution for 5 min at 37°C, then with 0.5 × SSC solution for 15 min, and finally with 0.2 × SSC solution for 15 min. The blocking solution was removed, and then anti-DIG biotin-labeled mouse antibody was added and incubated at 37°C for 1 h. This was followed by a 20-min incubation with a streptavidin-biotin complex and biotin-labeled peroxidase. Finally, diaminobenzidine reagent was used for color development, and the nuclei were stained with hematoxylin.

The staining scores were evaluated by two independent observers blinded to the clinical parameters based on the staining intensity (SI) and the percentage of positively stained area of tumor cells in relation to the whole tissue area (PR) [11]. The SI was scored from 0 to 3: 0 = no staining; 1 = weak staining; 2 = moderate staining; and 3 = strong staining. The PR was scored from 1 to 4: 1 = 0%-25%; 2 = 26%-50%; 3 = 51%-75%; and 4 = 75%-100%. The PR and the SI were multiplied to obtain a weighted score for each patient. A score of 8-12 indicated high expression, and a score of 0-7 indicated low expression.

Statistical analysis

The data were analyzed using SPSS 20.0 and GraphPad Prism 5 software. Quantitative data were presented as mean ± standard deviation. Categorical variables were presented as counts and percentages [*n* (%)]. To analyze time-course experiments with serial measurements, two-way repeated-measures analysis of variance (ANOVA) was performed to determine the overall group effect and group-by-time interaction. Differences between two groups were analyzed using Student *t* test, whereas comparisons among multiple groups were evaluated using one-way ANOVA.

The associations between miR-4286 expression levels and clinicopathological characteristics were evaluated using the χ^2 test or Fisher's exact test (applied when the expected cell frequencies were < 5). The optimal cutoff for age

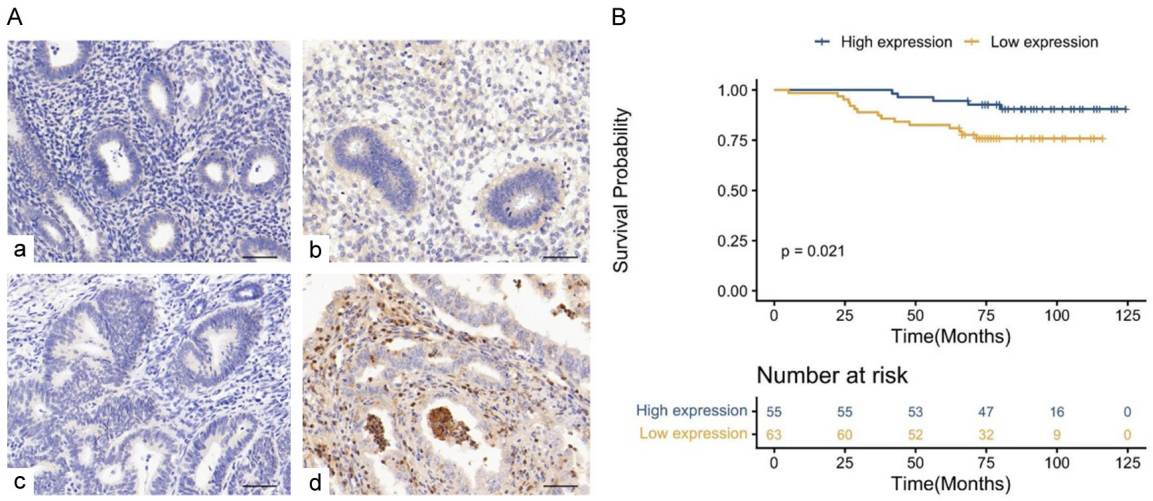

Figure 1. Clinicopathological features related to the expression of miR-4286. (A) Expression of miR-4286 in EC: (a and b) normal endometrium; (c and d) EC tissue (original magnification 200×), scale = 20 μm. (B) Kaplan-Meier survival analysis of the overall survival of 118 patients with EC based on the expression level of miR-4286.

Table 1. MiR-4286 expression in EC compared with normal endometrial tissue

Group	*N*	miR-4286 expression		*P*
		Low	High	
Cancer	152	90 (59.2)	62 (40.8)	0.005
Normal	43	15 (34.9)	28 (65.1)	

The χ^2 test was used to calculate miR-4286 expression in EC and normal endometrial samples.

grouping was based on clinical convention (< 50 vs ≥ 50 years). The miR-4286 expression level (high vs low) was classified according to the ISH scoring system as detailed in Section 2.17. No adjustment for multiple comparisons was applied for the baseline clinicopathological correlation analyses because these were exploratory in nature.

Survival analysis was conducted using Kaplan-Meier survival analysis. The median follow-up time was calculated using the reverse Kaplan-Meier method. The primary endpoint was overall survival (OS), defined as the time from the date of surgery to the date of death from any cause. Patients were censored if they were still alive at the date of the last follow-up or if they were lost to follow-up during the study period. Their data contributed to the "number at risk" until the point of their last known contact.

Univariate Cox proportional-hazards (PH) regression analyses were performed for all candidate independent variables to identify factors significantly associated with the outcome. Variables with a *P* value < 0.05 in the univariate analysis were subsequently included in a multivariable Cox regression model. Based on this multivariable model, backward stepwise selection using the Akaike Information Criterion was further employed to iteratively remove variables with minimal contribution, ultimately retaining factors with independent statistical significance. Reference categories for categorical variables were explicitly defined (FIGO stage I and high miR-4286 expression served as reference groups). The analysis was performed on complete-case data; no imputation was applied for missing clinical variables. The final model reported the hazard ratio (HR) and 95% confidence interval (95% CI) for each variable. The PH assumption was verified using Schoenfeld residuals. All statistical analyses were conducted using R software (version 4.5.2). The standards for determining statistical significance were as follows: $^{*}P < 0.05$, $^{**}P < 0.01$, and $^{***}P < 0.001$.

Results

Clinicopathological characteristics of patients with EC with miR-4286 expression

In situ hybridization demonstrated a low expression level of miR-4286 in EC (**Figure 1A**). Among 152 EC tumor samples, 59.2% (90/152) of cases exhibited low miR-4286 expres-

Table 2. Correlations between clinicopathological characteristics of patients and miR-4286 expression in EC

Characteristics	*N*	miR-4286 expression (%)		*P*
		High	Low	
Age				
< 50	40	16 (40.0)	24 (60.0)	0.906
≥ 50	112	46 (41.1)	66 (58.9)	
Pathological type				
Adenocarcinoma	144	59 (41.0)	85 (59.0)	0.845
Other	8	3 (37.5)	5 (62.5)	
Histological grading				
G1	48	22 (45.8)	26 (54.2)	0.468
G2	70	29 (41.4)	41 (58.6)	
G3	34	11 (32.4)	23 (67.6)	
FIGO stage				
I	115	54 (47.0)	61 (53.0)	0.023
II	18	6 (33.3)	12 (66.7)	
III	17	2 (11.8)	15 (88.2)	
IV	2	0	2 (100.0)	
Menopausal status				
Postmenopausal	105	46 (43.8)	59 (56.2)	0.258
Premenopausal	47	16 (34.0)	31 (66.0)	
Lymph node status				
Positive	17	2 (11.8)	15 (88.2)	0.010
Negative	135	60 (44.4)	75 (55.6)	
Myometrial invasion depth				
≥ 1/2	63	16 (25.4)	47 (74.6)	0.001
< 1/2	89	46 (51.7)	43 (48.3)	

P values were calculated using the χ^2 test or Fisher's exact test.

sion (**Table 1** and Figure S1). The clinical characteristics of patients with EC are summarized in **Table 2**. Further analysis revealed an association of the expression level of miR-4286 with FIGO staging ($P = 0.023$), lymph node metastasis ($P = 0.010$), and depth of myometrial infiltration ($P = 0.001$) in patients with EC, yet no significant correlations were observed with patients' age, menopausal status, histological grade, or pathological type (all $P > 0.05$).

Prognostic value of miR-4286 in EC

Kaplan-Meier survival analysis and Cox PH regression models were performed to evaluate the clinical prognostic value of miR-4286 in EC. The median follow-up time for the entire cohort was 85.77 months (95% CI: 81.70-91.83 months). Kaplan-Meier survival analysis confirmed that patients with high miR-4286 expression had a significantly longer OS compared with those with low expression levels ($P = 0.021$, **Figure 1B**). Furthermore, the univariate analysis indicated that histological grading, FIGO stage, lymph node metastasis, depth of myometrial invasion, and expression of miR-4286 were also significantly correlated with patients' survival (all $P < 0.05$). After adjusting for these clinical variables in the multivariable Cox model, low miR-4286 expression remained an independent predictor of poor prognosis in patients with EC (HR = 3.794, 95% CI: 1.265-11.376, $P = 0.017$) (**Table 3**).

MiR-4286 inhibited EC cell proliferation in vitro and in vivo

To overexpress or knock down miR-4286 expression, we transfected EC cells (RL95-2 and HEC-1-B) with miR-4286 mimics or an inhibitor and assessed miR-4286 assessed by qRT-PCR (**Figure 2A**). The biological functions of miR-4286 were analyzed employing MTT cell proliferation assays (**Figure 2B**) and G1/S cell cycle phase transition analyses using EdU incorporation assays. MTT analysis revealed significant main effects for both treatment group ($P < 0.001$) and time ($P < 0.001$), as well as a significant group × time interaction ($P < 0.001$). Both cell proliferation detected by MTT assays and cycle phase transition functions detected by EdU assays were inhibited after miR-4286-mimic transfection (**Figure 2C**). However, the miR-4286 inhibitor showed the opposite results; it promoted cell proliferation and G1/S cell cycle phase transition.

Moreover, we injected EC cells into nude mice and intratumorally injected miR-4286 agomirs to examine their effects on *in vivo* tumorigenesis. Consistent with *in vitro* data, the mice injected with miR-4286 agomirs had smaller tumor burdens; the average tumor weight was 0.03 g for RL95-2 cells and 0.11 g for HEC-1-B cells ($P < 0.05$, **Figure 3A**). IHC analyses revealed a decrease in Ki-67 and PCNA protein expression levels in tumor tissues expressing

Table 3. Summary of univariate and multivariable Cox regression analyses of overall survival duration

Parameter	Univariate analysis			Multivariable analysis		
	P	HR	95% CI	*P*	HR	95% CI
Age						
< 50 versus ≥ 50	0.837	0.904	0.347-2.354			
Histological grading						
G1 versus G2	0.026	10.289	1.328-79.708			
G1 versus G3	0.006	18.985	2.373-151.874			
FIGO stage						
I versus II	0.014	4.371	1.342-14.242	0.038	3.507	1.07-11.496
I versus III	< 0.001	23.439	8.447-65.039	< 0.001	31.482	10.073-98.394
Menopausal status						
Premenopausal versus Postmenopausal	0.628	0.797	0.318-1.997			
Lymph node status						
Negative versus positive	0.026	0.248	0.073-0.848			
Depth of myometrial invasion						
< 50% versus ≥ 50%	0.001	4.965	1.978-12.462			
MiR-4286 expression						
Low versus high	0.029	3.111	1.127-8.588	0.017	3.794	1.265-11.376

miR-4286 agomirs (**Figure 3B**). Thus, miR-4286 overexpression reduced *in vivo* xenograft growth.

We also assessed PI3K/Akt-related protein levels following miR-4286 modulation in EC cells. We found that miR-4286 overexpression decreased p-PI3K and p-Akt protein levels and increased p21 protein levels; the miR-4286-inhibitor showed the opposite results (**Figures 3C** and S2).

MiR-4286 inhibited EC cell migration, invasion, and metastasis in vitro and in vivo by suppressing the EMT pathway

Transwell and Boyden chamber assays were employed to assess the impact of miR-4286 on cell migration and invasion. After transfection, the invasiveness significantly decreased in miR-4286-overexpressing EC cells compared with negative controls ($P < 0.001$, **Figure 4A** and **4B**). Thus, miR-4286 overexpression reduced EC cell migration and invasion *in vitro*.

Next, we injected EC cells under the liver capsule of mice and then intraperitoneally injected the mice with miR-4286 agomirs to examine the effects of miR-4286 on EC metastasis. As shown in **Figure 4C**, the mice injected with miR-4286 agomirs had smaller tumor burdens in the liver and no peritoneal metastasis, whereas negative control mice had a larger tumor burden. Moreover, the percentage of mice with peritoneal metastasis was 66.67% (4/6) for RL95-2 cells and 83.3% (5/6) for HEC-1-B cells. IHC showed an increase in E-cadherin expression and a decrease in N-cadherin expression in liver tissue expressing miR-4286 agomirs (**Figure 4D**). Thus, miR-4286 overexpression decreased *in vivo* intrahepatic metastasis compared with that in controls.

We also examined EMT pathway proteins to characterize migration, invasion, and metastasis mechanisms in EC cells. N-cadherin, Vimentin, and Slug expression levels were downregulated, but E-cadherin expression level was upregulated in miR-4286-overexpressing EC cells. The trend was opposite in EC cells treated with the miR-4286 inhibitor (**Figures 5** and S2).

MiR-4286 directly targeted SNAI1

Using the miRPathDB and TargetScan algorithms, *SNAI1* was recognized as a direct target of miR-4286 (**Figure 6A**). The overexpression of miR-4286 in EC cell lines resulted in decreased levels of both *SNAI1* mRNA and protein (**Figure 6B** and **6C**). Besides, IHC analysis of xenografts derived from RL95-2 and HEC-1-B cells revealed that Snail expression was downregulated in cells with miR-4286 overexpression, which was consistent with the *in vitro* results (**Figure 6D**). Moreover, the luciferase reporter assays indicated a significant

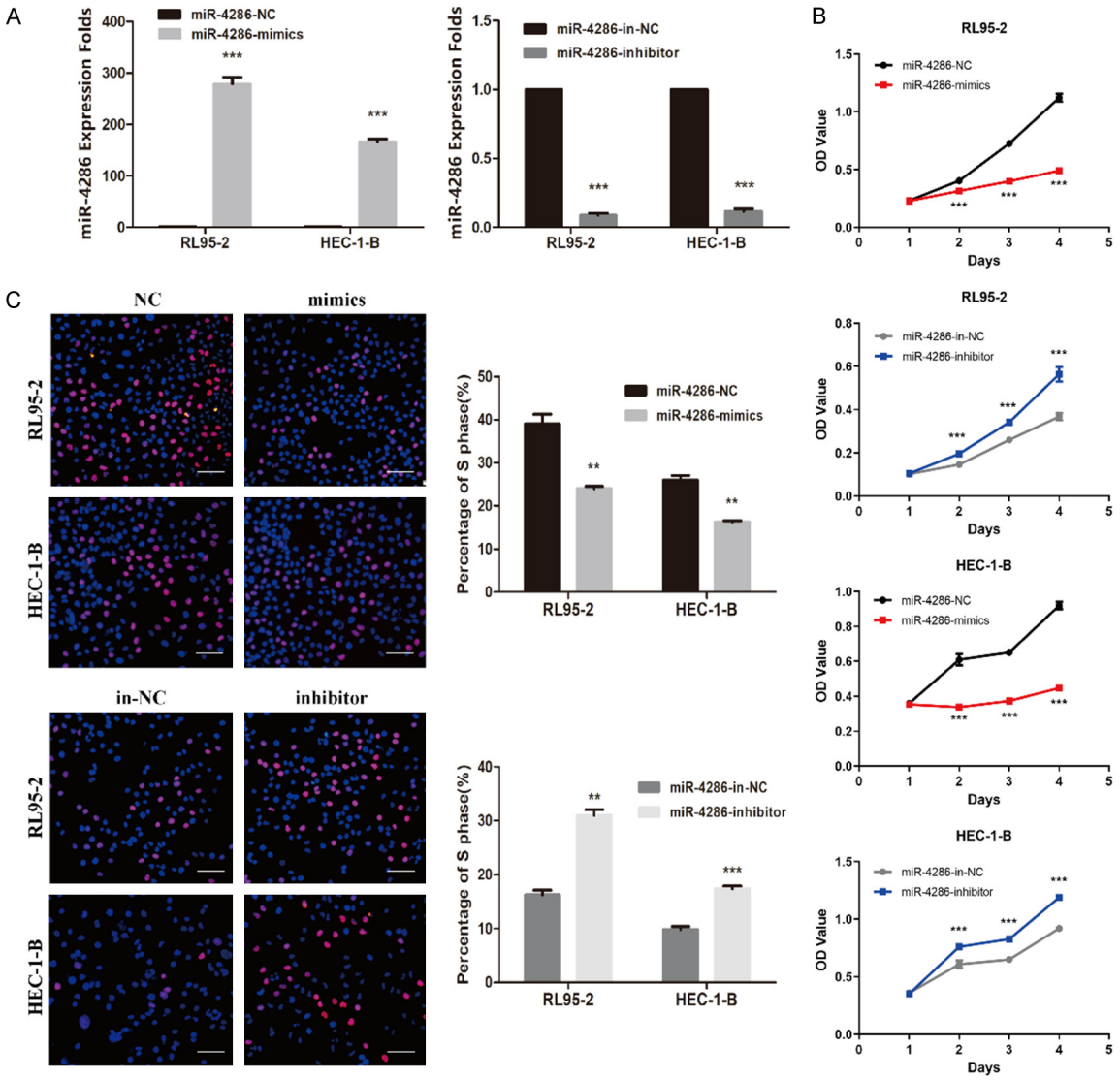

Figure 2. MiR-4286 inhibited EC cell proliferation *in vitro*. A. MiR-4286 was overexpressed or knocked down after transfection with mimics or an inhibitor. B. MTT assay data in miR-4286 overexpression or knockdown cells. Statistical significance across time points was determined using two-way repeated-measures ANOVA. C. EdU incorporation assays in miR-4286 overexpression or knockdown cells ($^{**}P < 0.01$, and $^{***}P < 0.001$).

decline in luciferase activity in cells carrying the wild-type *SNAI1* 3'-UTR when co-transfected with miR-4286 mimics ($P < 0.001$), whereas the opposite outcome was observed with the miR-4286 inhibitor ($P < 0.001$) (**Figure 6E**). Taken together, miR-4286 exerted an inhibitory effect on EC by directly repressing Snail expression.

We transiently transfected *SNAI1* siRNA into EC cells. Western blotting showed reduced Snail, p-PI3K and p-Akt levels and increased p21 expression following SNAI1 knockdown (**Figures 6F** and S3). Additionally, EMT-associated N-cadherin, Vimentin, and Slug expression was reduced but E-cadherin expression was induced after *SNAI1* siRNA transfection (**Figures 6G** and S3). These Western blot results were consistent with miR-4286 overexpression data. In SNAI1-transfected EC cells, co-transfection with miR-4286 mimics reduced Snail protein levels, MTT readouts, and invasive cell numbers compared with SNAI1 transfection alone (**Figure 6H-J**). Collectively, these findings implied that *SNAI1* was a direct target of miR-4286 mediating EMT signaling and that miR-

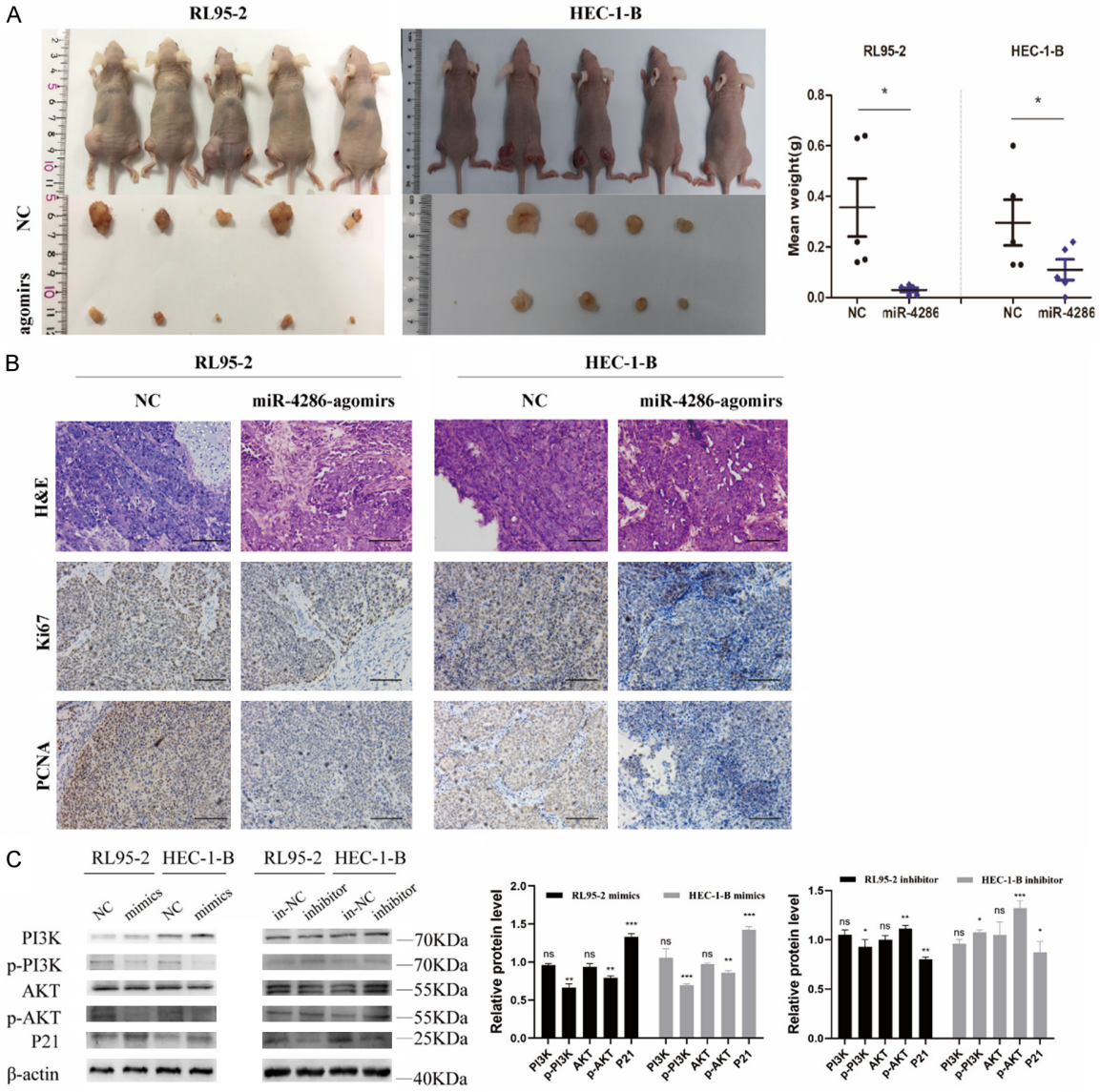

Figure 3. Effects of miR-4286 on xenograft growth and PI3K/Akt-related protein levels in EC cells. A. MiR-4286 overexpression reduced *in vivo* xenograft growth. B. Representative hematoxylin-eosin and immunohistochemistry staining of *Ki-67* and *PCNA* in xenografts (original magnification 200×). Scale bar = 20 μm. C. Western blotting analysis of PI3K, p-PI3K, Akt, p-Akt, and p21 expression after miR-4286 overexpression or knockdown ($^{*}P < 0.05$, $^{**}P < 0.01$, $^{***}P < 0.001$; ns: not significant).

4286 overexpression was associated with suppression of PI3K/Akt signaling and cell cycle regulation in EC.

p53 activated miR-4286 transcription by binding to its promoter region

To elucidate the regulation of miR-4286 expression, we used the JASPAR open-access database to examine a 2-kb region upstream of the transcription initiation site of miR-4286. This analysis revealed three potential p53-binding sites in the miR-4286 promoter region, with their positions at -1361 to -1347, -991 to -970, and -570 to -556 (**Figure 7A**). Next, we applied qRT-PCR to determine whether p53 controlled miR-4286 expression. The results showed a significant increase in miR-4286 expression in EC cells with *TP53* overexpression (**Figure 7B**), suggesting that p53 functioned as an upstream regulator of miR-4286 expression. To determine which predicted binding sites mediated p53 recruitment, ChIP-qPCR was performed across three potential

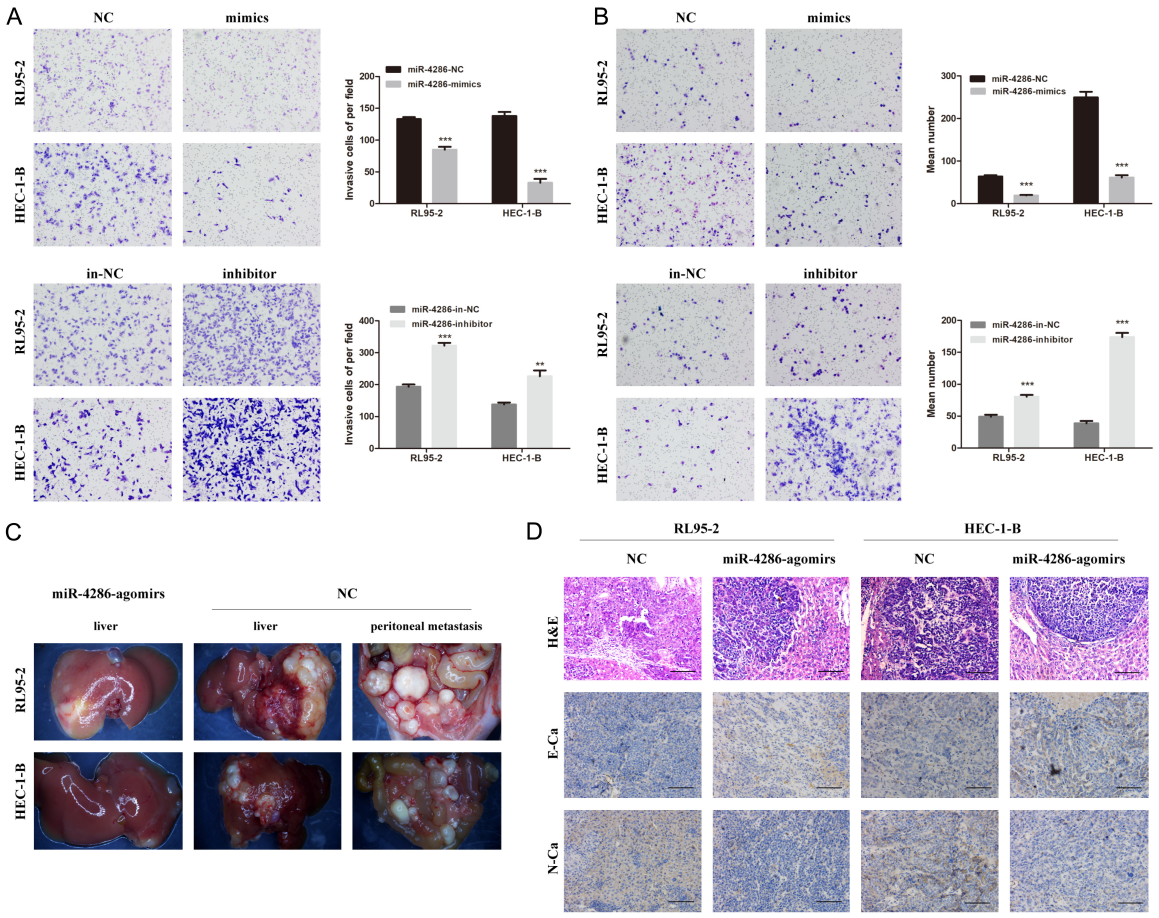

Figure 4. MiR-4286 suppressed the migration, invasion, and metastasis of EC cells both *in vitro* and *in vivo*. A. Transwell assays performed in EC cells with miR-4286 overexpression or knockdown. B. Boyden assays conducted in EC cells with miR-4286 overexpression or knockdown. C. Overexpression of miR-4286 reduced metastatic burden *in vivo*. D. Representative hematoxylin-eosin and immunohistochemical staining of E-cadherin and N-cadherin in liver tissue (original magnification 200×). The scale bar corresponds to 20 μm (***P* < 0.01, ****P* < 0.001).

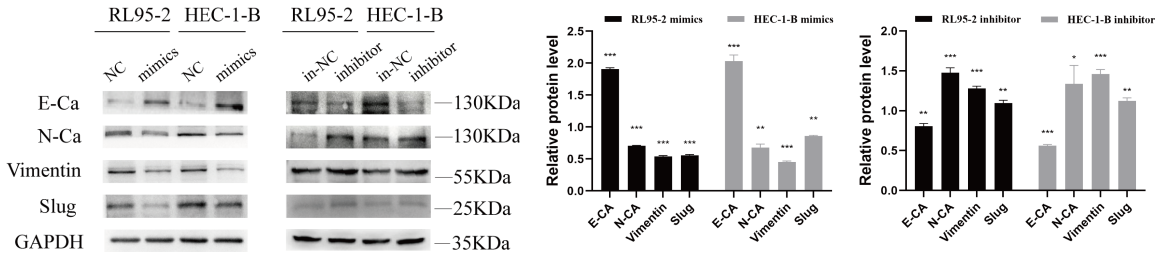

Figure 5. MiR-4286 suppressed malignant phenotypes by suppressing the EMT pathway. Western blotting analysis of E-cadherin, N-cadherin, Vimentin, and Slug expression in the EMT pathway after miR-4286 overexpression or knockdown (**P* < 0.05, ***P* < 0.01, and ****P* < 0.001).

p53-binding sites (P1, P2, and P3) within the promoter region. ChIP-qPCR analysis revealed significant p53 enrichment specifically at the P1 site, whereas no binding enrichment was detected at the P2 and P3 sites (**Figure 7C**). Consequently, ChIP-PCR analysis confirmed that p53 bound specifically to P1 areas of the miR-4286 promoter in EC cells (**Figure 7D**).

The EMSA was used to analyze the functional activity of the ChIP-positive P1 site (-570 to -556). As shown in **Figure 7E**, when the nuclear

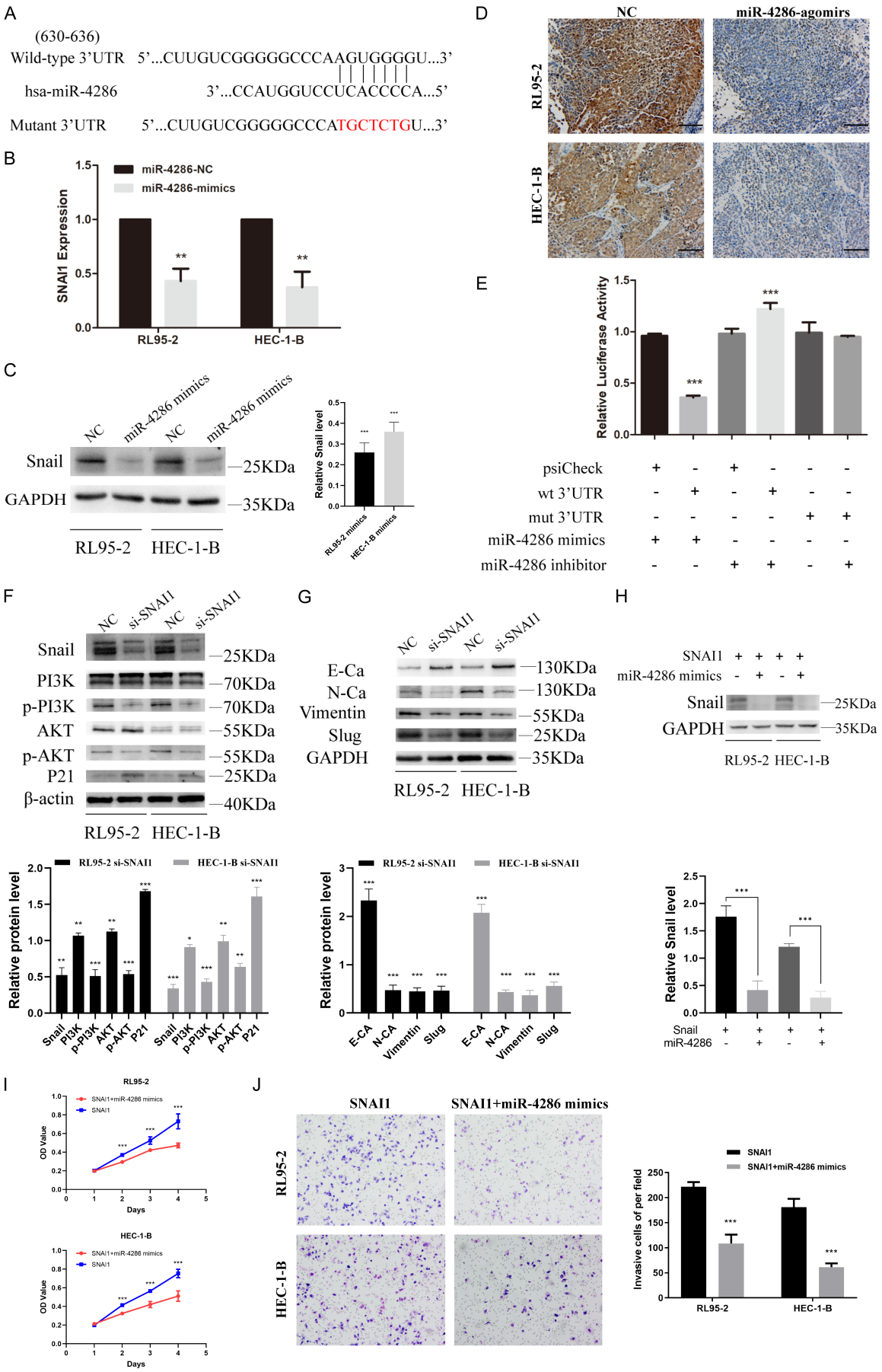
A
(630-636)
Wild-type 3'UTR 5'...CUUGUCGGGGGCCCAAGUGGGGU...3'
hsa-miR-4286 3'...CCAUGGUCCUCACCCCA...5'
Mutant 3'UTR 5'...CUUGUCGGGGGCCCATGCTCTGU...3'
B
miR-4286-NC
miR-4286-mimics
SNAI1 Expression
RL95-2
HEC-1-B
C
NC
miR-4286 mimics
Snail
GAPDH
25KDa
35KDa
RL95-2 HEC-1-B
Relative Snail level
RL95-2 mimics
HEC-1-B mimics
D
NC
miR-4286-agomirs
RL95-2
HEC-1-B
E
Relative Luciferase Activity
psiCheck
wt 3'UTR
mut 3'UTR
miR-4286 mimics
miR-4286 inhibitor
F
si-SNAI1
Snail
PI3K
p-PI3K
AKT
p-AKT
P21
β-actin
25KDa
70KDa
55KDa
40KDa
RL95-2 HEC-1-B
RL95-2 si-SNAI1
HEC-1-B si-SNAI1
Relative protein level
G
E-Ca
N-Ca
Vimentin
Slug
130KDa
RL95-2 HEC-1-B
H
SNAI1
miR-4286 mimics
Relative Snail level
I
RL95-2
HEC-1-B
SNAI1+miR-4286 mimics
SNAI1
OD Value
Days
J
SNAI1
SNAI1+miR-4286 mimics
Invasive cells of per field

Figure 6. MiR-4286 directly targeted *SNAI1*. A. Bioinformatics miR-4286-binding prediction sites in the *SNAI1* 3'-untranslated region. B. *SNAI1* mRNA expression detected using qRT-PCR after miR-4286 overexpression. C. Western blotting analysis of Snail protein levels. GAPDH served as a loading control. D. Snail immunohistochemistry staining in xenografts from miR-4286-agomirs expressing EC nude models. Scale bar = 20 μm. E. Luciferase reporter assays were used to validate that miR-4286 directly targeted *SNAI1*. F. Western blotting analysis of PI3K, p-PI3K, Akt, p-Akt, and p21 protein levels following *SNAI1* knockdown. β-actin acted as the loading control. G. Western blotting was employed to analyze the expression of E-cadherin, N-cadherin, Vimentin, and Slug in the EMT pathway following *SNAI1* knockdown. GAPDH served as a loading control. H. Downregulation of Snail expression in *SNAI1*-overexpressing EC cells detected using Western blotting following transfection with miR-4286 mimics. I. MTT assays comparing SNAI1-transfected EC cells with and without co-transfection with miR-4286 mimics (two-way repeated-measures ANOVA). J. Transwell invasion assays comparing SNAI1-transfected EC cells with and without co-transfection with miR-4286 mimics ($^{*}P < 0.05$, $^{**}P < 0.01$, and $^{***}P < 0.001$).

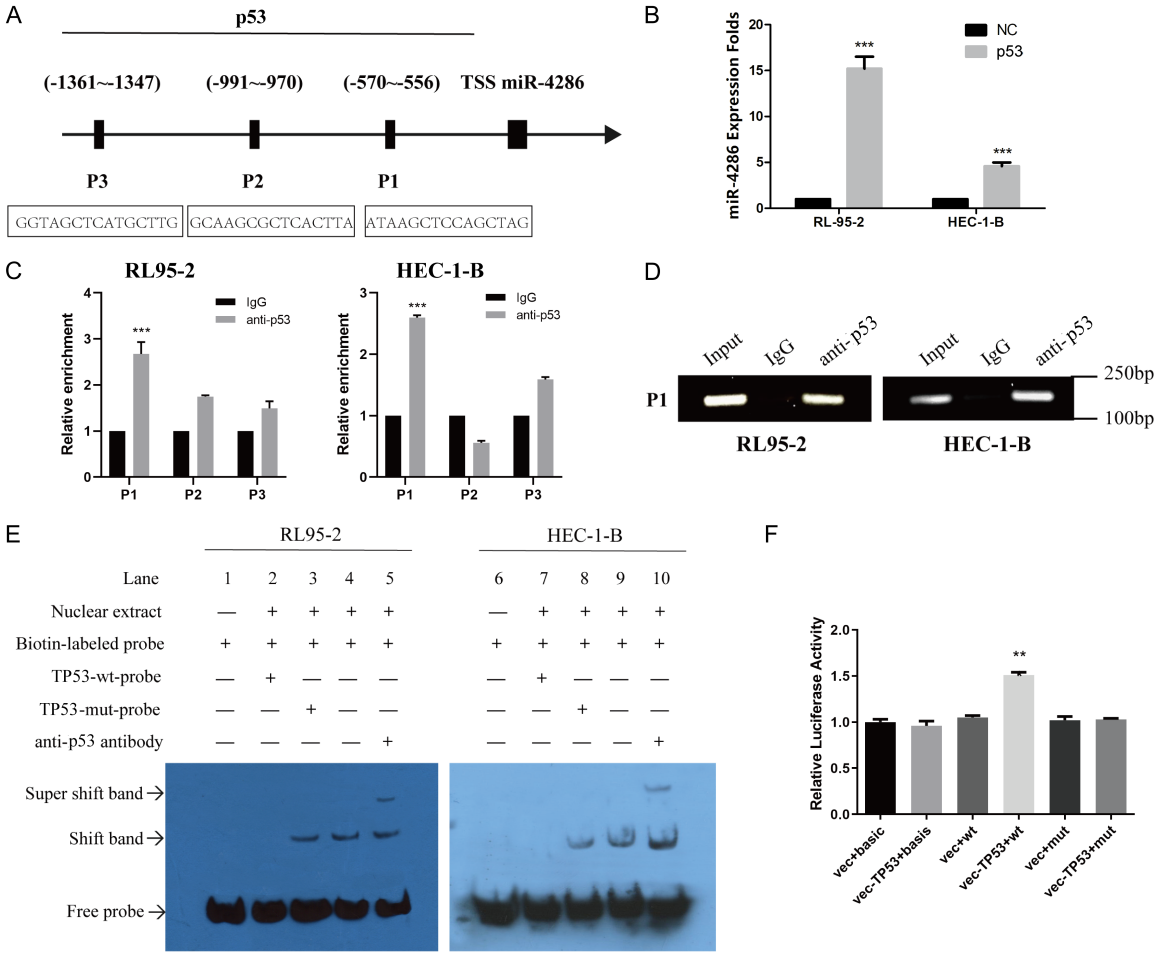

Figure 7. p53 activated miR-4286 transcription by binding to its promoter region. A. Schematic showing miR-4286 promoter regions with three putative p53-binding sites (P1, P2, and P3). B. MiR-4286 expression detected using qRT-PCR after *TP53* overexpression. C. ChIP-qPCR assays evaluating p53-binding enrichment at P1, P2, and P3 sites. D. PCR gel demonstrating the amplification of the p53-binding site P1 following ChIP with an antibody targeting p53. IgG served as a negative control. E. EMSA confirming direct *in vitro* binding of p53 to the ChIP-validated P1 binding sequence. When nuclear extracts from EC cells were incubated with a biotin-labeled probe, shifted bands were detected in lanes 4 and 9. In contrast, no shifted bands appeared on adding an unlabeled wild-type *TP53* probe as a binding competitor (lanes 2 and 7). Meanwhile, super-shifted bands emerged when the p53 antibody was present (lanes 5 and 10). F. Luciferase reporter assays were used to verify that p53 activated the transcription of miR-4286 by binding to its promoter region ($^{***}P < 0.001$).

extracts from EC cells were incubated with a biotin-labeled probe, shifted bands were detected in lanes 4 and 9. In contrast, no shifted bands were observed when an unlabeled

wild-type *TP53* probe was added as a binding competitor (lanes 2 and 7). Super-shifted bands emerged when the p53 antibody was present (lanes 5 and 10). Thus, p53 bound directly to the miR-4286 promoter sequence and modulated its expression. To verify these findings, we used a dual-luciferase reporter assay system to evaluate miR-4286 transcriptional activity. Compared with the mutant miR-4286 promoter, HEK293T cells transfected with the wild-type miR-4286 promoter together with *TP53* exhibited a marked increase in luciferase activity (**Figure 7F**).

Discussion

EC is an epithelial malignant tumor characterized by the abnormal proliferation of endometrial cells, with invasion and metastasis representing the primary drivers of disease progression [13]. MiRNA research has gained immense interest in recent years due to the key functional roles played by these molecules in tumor progression. Ravegnini *et al*. recently proposed that integrating TCGA data on EC with miR-499a-5p subgroups enhanced patient stratification and supported personalized treatment approaches [14]. Furthermore, specific miRNAs, such as miR-205, miR-146a, and miR-1260b, have emerged as potential biomarkers for precancerous lesions [15], whereas miR-21 expression has been identified as an independent predictor of progression-free survival [16]. These miRNA studies have introduced promising novel candidates for targeted therapy in EC. Our study found that miR-4286 was significantly downregulated in EC tissue and associated with the FIGO stage, lymph node status, and myometrial invasion depth, all of which are established indicators of a poor prognosis.

Accumulated evidence indicates that microRNAs can exert tissue-specific functions in human malignancies. However, the opposing oncogenic versus tumor-suppressive actions of miR-4286 across various cancer types warrant deeper mechanistic consideration. The context-dependent dual role of miR-4286 may be attributed to the specific tumor microenvironment, the mutation status of upstream regulators (e.g., p53/NF-κB), and the distinct expression landscapes of downstream target genes in different tissues. For instance, activated by NF-κB, miR-4286 overexpression increased cell proliferation and motility by targeting *BZRAP1* in *Helicobacter pylori*-associated gastric cancer [17]. Additionally, bioinformatics pan-cancer survival analyses suggested that lower miR-4286 expression was associated with poorer survival in patients with lung adenocarcinoma and EC [18]. This upstream transcriptional wiring and tissue-specific target site availability determine whether miR-4286 manifests as a tumor suppressor or an oncogene in a given cellular context. However, the specific biological mechanisms of action of miR-4286 in EC remain unexplored. We conducted overexpression and knockdown assays in EC cell lines to characterize the molecular functions of miR-4286 in EC. Our results showed that upregulation of miR-4286 inhibited proliferation, migration, and invasion of EC cells both *in vitro* and *in vivo.* These findings suggested that miR-4286 functioned as a tumor suppressor in EC.

Although bioinformatic algorithms suggest multiple candidate targets for miR-4286, our functional rescue data showed that re-expressing *SNAI1* alone was sufficient to substantially reverse the antiproliferative and anti-invasive phenotypes induced by miR-4286. This indicated that SNAI1 served as the central functional driver of the p53/miR-4286 axis in EC pathogenesis. A previous study revealed that genetic polymorphisms in *SNAI1* were associated with EC susceptibility [19]. The EMT is a key step in cancer pathogenesis [20]. As a primary regulator of EMT, Snail, a hallmark of cancer pathogenesis, facilitates tumor survival by conferring resistance to apoptosis and promoting invasion and metastasis [21-23]. EMT is characterized by the downregulation of E-cadherin expression, which may be suppressed by Snail [24, 25]. Studies have shown that reduced E-cadherin expression and higher Snail expression in EC tissue had an impact on EC prognosis [26, 27]. In our study, *in vitro* experiments with miR-4286 overexpression and miR-4286 knockdown showed that miR-4286 overexpression enhanced E-cadherin protein expression but reduced N-cadherin, Vimentin, and Slug expression. Furthermore, *SNAI1* knockdown reduced phosphorylated PI3K and Akt protein levels in both EC cell lines. However, the present experiments do not establish the molecular mechanism underlying

these changes. The relationship between SNAI1 and PI3K/Akt signaling therefore requires further mechanistic investigation.

The binding of transcription factors to sequences in upstream promoter regions of miRNA genes regulates miRNA expression [12]. Depending on the bioinformatics datasets, p53 may be linked to the transcriptional upregulation of miR-4286. As the guardian of the genome, p53 plays key roles in destroying cancer cells via apoptosis [28]. The p53 protein is a well-known transcription factor that regulates several cellular functions, such as cell cycle arrest, DNA repair, senescence, and apoptosis [29]. However, *TP53* mutations are frequently observed in EC, particularly within the TCGA copy-number high subgroup, which is characterized by p53 dysfunction and poor clinical outcomes [30-33]. In this study, we tested the hypothesis that wild-type p53 suppresses EC carcinogenesis by regulating miR-4286. Our bioinformatics analysis identified p53 as a potential transcription factor. Subsequent qRT-PCR analysis confirmed that p53 upregulated miR-4286 expression. In this study, we used two EC cell lines with distinct *TP53* genetic backgrounds: RL95-2 (*TP53* wild-type) and HEC-1-B (*TP53*-mutant). Our luciferase, ChIP, and EMSA assays confirmed that wild-type p53 protein directly bound to the promoter of miR-4286 to transactivate its expression. A key question arises regarding whether miR-4286 retains its tumor-suppressive capability in a p53-mutant or p53-deficient background. Our results provide clear evidence that p53 status dictates upstream miR-4286 transcription but does not impair its downstream functional capacity. Specifically, in *TP53*-mutant HEC-1-B cells with downregulation of endogenous miR-4286 expression, exogenous restoration of miR-4286 (via mimics or agomirs) targeted *SNAI1*, repressing EMT and suppressing malignant phenotypes both *in vitro* and *in vivo*. This indicated that the RNA-induced silencing complex-mediated repression of SNAI1 by miR-4286 operated independently of functional p53. In clinical settings, EC tumors with wild-type p53, such as those in the TCGA copy-number low or NSMP subgroups, maintain an intact p53/miR-4286/*SNAI1* tumor-suppressive axis. Conversely, in *TP53*-mutant ECs frequently observed in high-grade endometrioid and serous carcinomas within the TCGA copy-number high subgroup, the loss of functional wild-type p53 leads to the transcriptional silencing of miR-4286, thereby permitting Snail upregulation and driving EMT activation. As miR-4286 retains its intrinsic potency in p53-mutant contexts, the exogenous delivery of miR-4286 represents a promising bypass therapeutic strategy to re-establish tumor suppression in p53-deficient EC. Although the ectopic restoration of wild-type p53 in HEC-1-B cells re-established miR-4286 expression, a major study limitation was the reliance on exogenous wild-type p53 expression in a mutant baseline. Future investigations employing endogenous p53 knock-in/knock-out systems can further clarify the subtle dominant-negative effects of specific p53 mutants on miR-4286 transcription.

Limitations

This study had several limitations. First, the study used *p14ARF* as the reference gene for qRT-PCR. This is because the transcription levels of *p14ARF* can vary with p53 overexpression or cellular stress, potentially causing normalization bias. However, major downstream signaling changes and target proteins, such as SNAI1, phosphorylated PI3K, phosphorylated Akt, and EMT markers, were confirmed via Western blotting, using GAPDH and β-actin as controls. Second, the study did not establish the molecular mechanism linking SNAI1 to the observed changes in phosphorylated PI3K and Akt levels or determine whether PI3K/Akt signaling is required for the phenotypic effects of miR-4286. Third, the retrospective design of the study led to missing detailed clinical data, such as hormone receptor status, treatment regimens, and TCGA molecular subtypes, for the TMA cohort. Although we found strong associations between miR-4286 expression and clinical outcomes, multivariate analyses by molecular subtypes or treatments could not be conducted. Finally, as a nude mouse model lacks a fully functional immune system, we could not assess the effect of miR-4286 on the tumor immune microenvironment, highlighting the need for studies using immunocompetent mice.

Conclusions

Figure 8 presents a regulatory model summarizing our findings. MiR-4286 was identified as a tumor suppressor inhibiting EC progression. It

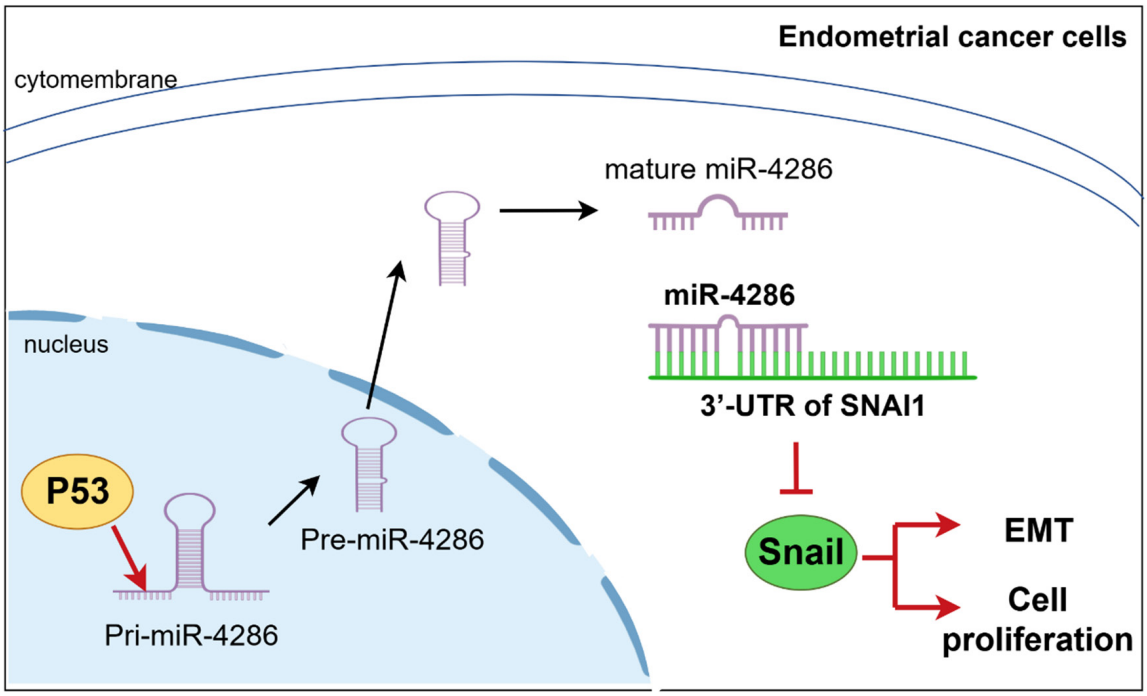

Figure 8. Schematic diagram of the p53/miR-4286/*SNAI1* signaling pathway in EC (By Figdraw).

inhibited EC cell proliferation, invasion, and metastasis both *in vitro* and *in vivo* by directly targeting *SNAI1* to inhibit EMT. miR-4286 overexpression and *SNAI1* knockdown were accompanied by changes in phosphorylated PI3K/Akt proteins in EC cells. This study provides novel insights into the molecular mechanisms underpinning EC.

Acknowledgements

The authors thank Editor Bar for its linguistic assistance during the preparation of this manuscript. This study was supported by the Natural Science Fund of Guangdong Province (Grant No. 2020A1515010087) and the Sanming Project of Medicine in Shenzhen (Grant No. SZSM202211020).

The patients provided their written informed consent to participate in this study.

Disclosure of conflict of interest

None.

Address correspondence to: Dr. Ping Jin, Shenzhen Maternity and Child Healthcare Hospital, Women and Children's Medical Center, Southern Medical University, No. 2004, Hongli Road, Shenzhen 518017, Guangdong, China. E-mail: pingjin68@smu.edu.cn; Dr. Suiqun Guo, The Third Affiliated Hospital of Southern Medical University, No. 183, Zhongshan Avenue, Guangzhou 510315, Guangdong, China. E-mail: guosuiqun@smu.edu.cn

References

[1] Siegel RL, Kratzer TB, Giaquinto AN, Sung H and Jemal A. Cancer statistics, 2025. CA Cancer J Clin 2025; 75: 10-45.

[2] Espinosa I, D'Angelo E and Prat J. Endometrial carcinoma: 10 years of TCGA (the cancer genome atlas): a critical reappraisal with comments on FIGO 2023 staging. Gynecol Oncol 2024; 186: 94-103.

[3] Forjaz G, Ries L, Devasia TP, Flynn G, Ruhl J and Mariotto AB. Long-term cancer survival trends by updated summary stage. Cancer Epidemiol Biomarkers Prev 2023; 32: 1508-1517.

[4] Ferragut Cardoso AP, Banerjee M, Nail AN, Lykoudi A and States JC. miRNA dysregulation is an emerging modulator of genomic instability. Semin Cancer Biol 2021; 76: 120-131.

[5] Smith ES, Whitty E, Yoo B, Moore A, Sempere LF and Medarova Z. Clinical applications of short non-coding RNA-based therapies in the era of precision medicine. Cancers (Basel) 2022; 14: 1588.

[6] Wang X, Jiang N, Yin W and Cui X. MicroRNAs as multifaceted regulators and therapeutic tar-

gets in ulcerative colitis. Front Immunol 2025; 16: 1697059.
[7] Li Z, Zhao S, Wang H, Zhang B and Zhang P. miR-4286 promotes prostate cancer progression by targeting the expression of SALL1. J Gene Med 2023; 25: e3127.
[8] Pochileev I, Fakirova A, Tashkova D, Gerdgikova A, Ilieva N, Serteva D, Shalamanova G, Ivanov H, Linev A and Dimova I. Upregulation of miR-4286 and miR-146a-5p in metastatic melanoma, revealed by multiplex expression analysis. Curr Issues Mol Biol 2026; 48: 279.
[9] Ho KH, Chen PH, Shih CM, Lee YT, Cheng CH, Liu AJ, Lee CC and Chen KC. miR-4286 is involved in connections between IGF-1 and TGF-β signaling for the mesenchymal transition and invasion by glioblastomas. Cell Mol Neurobiol 2022; 42: 791-806.
[10] Xiao YY, Lin L, Li YH, Jiang HP, Zhu LT, Deng YR, Lin D, Chen W, Zeng CY, Wang LJ, Chen SC, Jiang QP, Liu CH, Fang WY and Guo SQ. ZEB1 promotes invasion and metastasis of endometrial cancer by interacting with HDGF and inducing its transcription. Am J Cancer Res 2019; 9: 2314-2330.
[11] Liu Y, Wang Q, Guo Q, Zhu Y, Lin L, Yang C, Gong B, Yan W, Hou R, Tang Y, Wu X, Liu X, Zhou B, Fang W, Shu L and Guo S. FBXW7 directly ubiquitinates and degrades CTNNB1 mediating the suppression of ENKUR in endometrial cancer. Int J Biol Sci 2025; 21: 1801-1818.
[12] He T, Shen H, Wang S, Wang Y, He Z, Zhu L, Du X, Wang D, Li J, Zhong S, Huang W and Yang H. MicroRNA-3613-5p promotes lung adenocarcinoma cell proliferation through a RELA and AKT/MAPK positive feedback loop. Mol Ther Nucleic Acids 2020; 22: 572-583.
[13] Ren X, Liang J, Zhang Y, Jiang N, Xu Y, Qiu M, Wang Y, Zhao B and Chen X. Single-cell transcriptomic analysis highlights origin and pathological process of human endometrioid endometrial carcinoma. Nat Commun 2022; 13: 6300.
[14] Ravegnini G, De Leo A, Coada C, Gorini F, de Biase D, Ceccarelli C, Dondi G, Tesei M, De Crescenzo E, Santini D, Corradini AG, Tallini G, Hrelia P, De Iaco P, Angelini S and Perrone AM. Identification of miR-499a-5p as a potential novel biomarker for risk stratification in endometrial cancer. Front Oncol 2021; 11: 757678.
[15] Giglio S, Annibali V, Cirombella R, Faruq O, Volinia S, De Vitis C, Pesce M, Caserta D, Pettinato A, Fraggetta F and Vecchione A. miRNAs as candidate biomarker for the accurate detection of atypical endometrial hyperplasia/endometrial intraepithelial neoplasia. Front Oncol 2019; 9: 526.
[16] Sato K, Miyamoto M, Takano M and Tsuda H. MicroRNA-21 expression in cancer cells is an independent biomarker of progression-free survival of endometrioid endometrial carcinoma. Virchows Arch 2021; 479: 883-891.
[17] Tsai CC, Chen TY, Tsai KJ, Lin MW, Hsu CY, Wu DC, Tsai EM and Hsieh TH. NF-κB/miR-18a-3p and miR-4286/BZRAP1 axis may mediate carcinogenesis in Helicobacter pylori-associated gastric cancer. Biomed Pharmacother 2020; 132: 110869.
[18] An X, Ge J, Guo H, Mi H, Zhou J, Liu Y, Weiyue and Wu Z. Overexpression of miR-4286 is an unfavorable prognostic marker in individuals with non-small cell lung cancer. J Cell Biochem 2019; 120: 17573-17583.
[19] Yang L, Wang YJ, Zheng LY, Jia YM, Chen YL, Chen L, Liu DG, Li XH, Guo HY, Sun YL, Tian XX and Fang WG. Genetic polymorphisms of TGFB1, TGFBR1, SNAI1 and TWIST1 are associated with endometrial cancer susceptibility in Chinese Han women. PLoS One 2016; 11: e0155270.
[20] LeBleu VS and Thiery JP. The continuing search for causality between epithelial-to-mesenchymal transition and the metastatic fitness of carcinoma cells. Cancer Res 2022; 82: 1467-1469.
[21] Huber MA, Kraut N and Beug H. Molecular requirements for epithelial-mesenchymal transition during tumor progression. Curr Opin Cell Biol 2005; 17: 548-558.
[22] Nieto MA. The snail superfamily of zinc-finger transcription factors. Nat Rev Mol Cell Biol 2002; 3: 155-166.
[23] Ghafoor S, Garcia E, Jay DJ and Persad S. Molecular mechanisms regulating epithelial mesenchymal transition (EMT) to promote cancer progression. Int J Mol Sci 2025; 26: 4364.
[24] Rubtsova SN, Zhitnyak IY and Gloushankova NA. Dual role of E-cadherin in cancer cells. Tissue Barriers 2022; 10: 2005420.
[25] Wang L, Li S, Luo H, Lu Q and Yu S. PCSK9 promotes the progression and metastasis of colon cancer cells through regulation of EMT and PI3K/AKT signaling in tumor cells and phenotypic polarization of macrophages. J Exp Clin Cancer Res 2022; 41: 303.
[26] Comijn J, Berx G, Vermassen P, Verschueren K, van Grunsven L, Bruyneel E, Mareel M, Huylebroeck D and van Roy F. The two-handed E box binding zinc finger protein SIP1 downregulates E-cadherin and induces invasion. Mol Cell 2001; 7: 1267-1278.
[27] Li H, Wang J, Li L, Zhao L and Wang Z. Correction: expression of EMT-related genes in lymph node metastasis in endometrial cancer: a TCGA-based study. World J Surg Oncol 2023; 21: 97.

[28] Wang Y, Liang Y, Yang G, Lan Y, Han J, Wang J, Yin D, Song R, Zheng T, Zhang S, Pan S, Liu X, Zhu M, Liu Y, Cui Y, Meng F, Zhang B, Liang S, Guo H, Liu Y, Hassan MK and Liu L. Tetraspanin 1 promotes epithelial-to-mesenchymal transition and metastasis of cholangiocarcinoma via PI3K/AKT signaling. J Exp Clin Cancer Res 2018; 37: 300.

[29] Hibino E and Hiroaki H. Potential of rescue and reactivation of tumor suppressor p53 for cancer therapy. Biophys Rev 2022; 14: 267-275.

[30] Hernández Borrero LJ and El-Deiry WS. Tumor suppressor p53: biology, signaling pathways, and therapeutic targeting. Biochim Biophys Acta Rev Cancer 2021; 1876: 188556.

[31] Momeni-Boroujeni A, Dahoud W, Vanderbilt CM, Chiang S, Murali R, Rios-Doria EV, Alektiar KM, Aghajanian C, Abu-Rustum NR, Ladanyi M, Ellenson LH, Weigelt B and Soslow RA. Clinicopathologic and genomic analysis of TP53-mutated endometrial carcinomas. Clin Cancer Res 2021; 27: 2613-2623.

[32] Whelan K, Dillon M, Strickland KC, Pothuri B, Bae-Jump V, Borden LE, Thaker PH, Haight P, Arend RC, Ko E, Jackson AL, Corr BR, Ayoola-Adeola M, Wright JD, Podwika S, Smitherman C, Thomas S, Lightfoot M, Newton M, Washington C, Mullen M, Cosgrove C, Harsono AAH, Powell K, Herzog TJ, Salani R and Alvarez Secord A. TP53 mutation and abnormal p53 expression in endometrial cancer: associations with race and outcomes. Gynecol Oncol 2023; 178: 44-53.

[33] Slomovitz BM, Danziger N, Quintanilha JCF, Kelly AD, Li G, Podder V, Lin DI, Graf RP, Elvin JA and Herzog TJ. Validation of comprehensive genomic profiling for prognostic and potential therapeutic molecular classification of endometrial cancer. Int J Gynecol Cancer 2025; 35: 102107.

Table S1. The sequences of miR-4286 mimics, miR-4286 inhibitor and si-*SNAI1*

Gene		Sequence
miR-4286 mimic	sense	5'-ACCCCACUCCUGGUACC-3'
	anti-sense	3'-UGGGGUGAGGACCAUGG-5'
miR-4286 inhibitor	sense	5'-UGGGGUGAGGACCAUGG-3'
si-*SNAI1*	sense	5'-GGTGTGACTAACTATGCAA-3'

Table S2. The primers and probes used in this study

Gene		Sequence
U6	forward	5'-GGAACGATACAGAGAAGATTAGC-3'
	reverse	3'-TGGAACGCTTCACGAATTTGCG-5'
ARF	forward	5'-ATCTGTTTCACAGTCTGGGACG-3'
	reverse	3'-CCTGCTTGTTGGCAAATACC-5'
SNAI1	forward	5'-CTCGCTGCCAATGCTCATCT-3'
	reverse	3'-CCTTTCCCACTGTCCTCATCTG-5'
ChIP-p53-P1 binding sites	forward	5'-AGGGCTGAAGCTACTTGTCTT-3'
	reverse	3'-GCAATGGTCTCCTGGCAAAG-5'
ChIP-p53-P2 binding sites	forward	5'-AGCATGGATGAACCTTGAAGACA-3'
	reverse	3'-GACTACACCAGGGACCTCATATAAG-5'
ChIP-p53-P3 binding sites	forward	5'-GCGTGGTAGCTCATGCTTGTAAT-3'
	reverse	3'-CTCCTGGGCTCAAGTGATCCT-5'
EMSA	biotin-labeled probe	AACCTATAAGCTCCAGCTAGAAGGTTA
EMSA	wild-type competitor	AACCTATAAGCTCCAGCTAGAAGGTTA
EMSA	mutated competitors	AACCTTCGGATAGGTAGGTCAAGGTTA

Table S3. The antibodies used for Western blot, immunohistochemistry assays, ChIP, EMSA

Antibody	Company	Catalog number	Clone number	Host species	Molecular	
					Weight	Dilution
PI3K	Proteintech Group	20584-1-AP	N/A	Rabbit	110 kDa	1:1000
p-PI3K	Cell Signaling Technology	4228	Tyr458/Tyr199	Rabbit	60,85 kDa	1:1000
AKT	Proteintech Group	10176-2-AP	N/A	Rabbit	56-62 kDa	1:2000
p-AKT	Cell Signaling Technology	9611	N/A	Rabbit	60 kDa	1:2000
P21	Cell Signaling Technology	64016	N/A	Rabbit	21 kDa	1:1000
E-cadherin	Cell Signaling Technology	3195	24E10	Rabbit	135 kDa	1:1000
N-cadherin	Cell Signaling Technology	13116	D4R1H	Rabbit	140 kDa	1:1000
Vimentin	Cell Signaling Technology	5741	D21H3	Rabbit	57 kDa	1:1000
Snail	Cell Signaling Technology	3879	C15D3	Rabbit	29 kDa	1:1000
Slug	Cell Signaling Technology	9585	C19G7	Rabbit	30 kDa	1:1000
p53	Abcam	ab26	PAb 240	Mouse	53 kDa	10 μg/test
PCNA	Cell Signaling Technology	13110	D3H8P	Rabbit	36 kDa	1:4000
Ki-67	Cell Signaling Technology	9449	8D5	Mouse	36 kDa	1:5000
GAPDH	Cell Signaling Technology	5174	D16H11	Rabbit	37 kDa	1:1000
β-actin	Santa	sc-47778	C4	Mouse	43 kDa	1:1000
HRP-conjugated Goat Anti-Rabbit IgG (H+L)	Proteintech	SA00001-2	N/A	Goat	N/A	1:5000
HRP-conjugated Goat Anti-Mouse IgG (H+L)	Proteintech	SA00001-1	N/A	Goat	N/A	1:5000

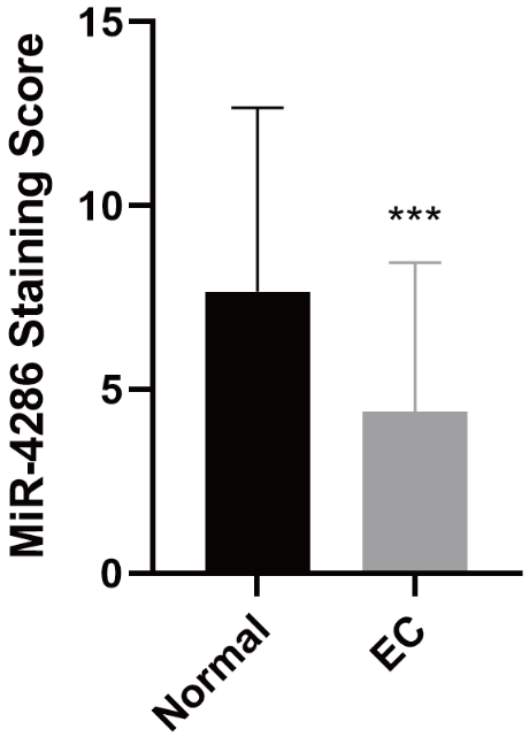

Figure S1. miR-4286 expression staining score of EC and normal samples.



Figure S2. WB original versions of **Figures 3** and **5**.

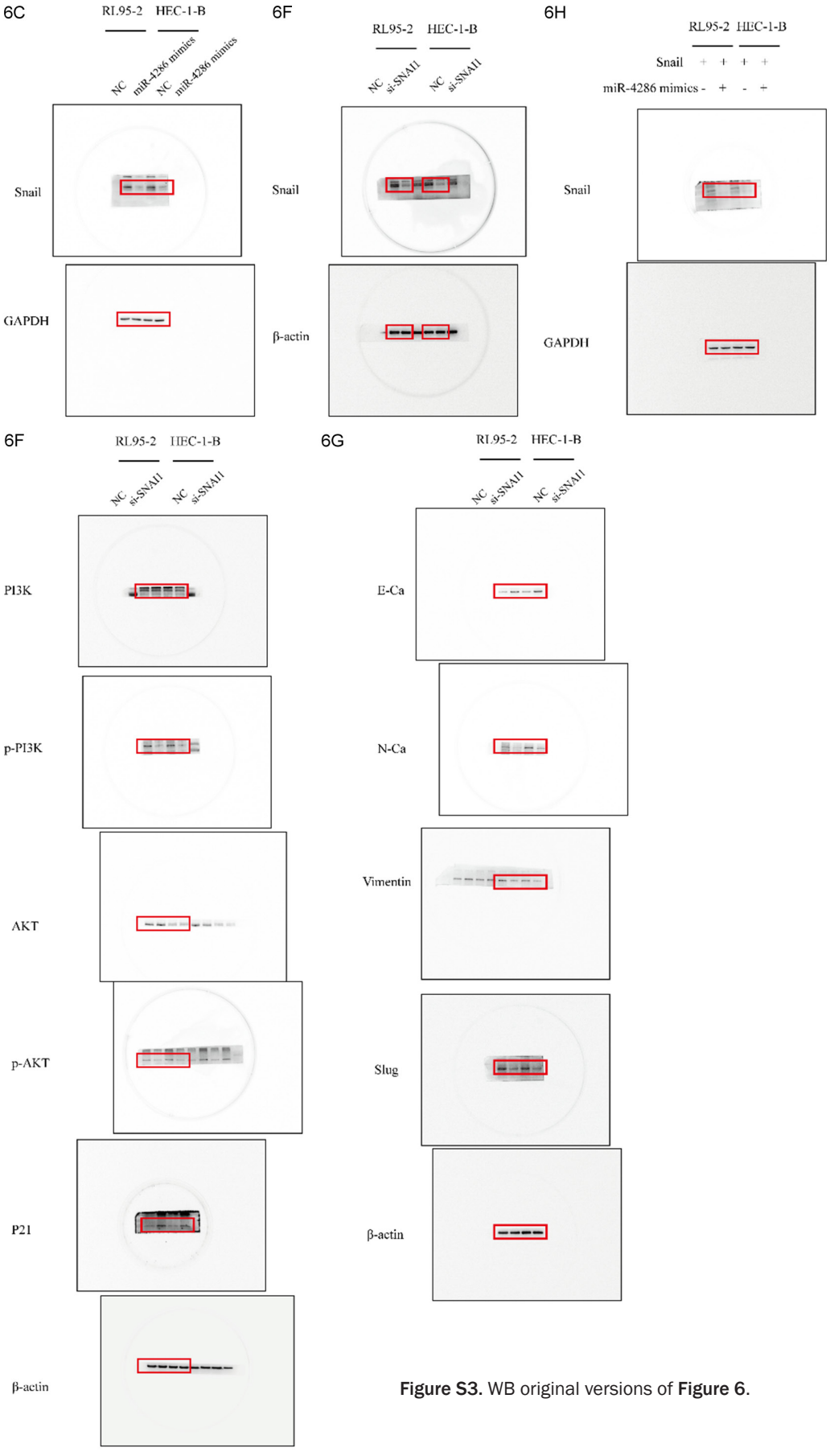

Figure S3. WB original versions of **Figure 6**.